Optimized compact fortified weight-prioritized convolutional network for swift skin lesion identification using dermoscopic images

R Priyanka Pramila[1*], R Subhashini[2]

1Research Scholar, School of Computing, Sathyabama Institute of Science and Technology, Chennai, India.
priyankastephen1702@gmail.com ; myresearchsub@gmail.com (R.P.P.)
2Department of Computer Science Engineering, SRM Institute of Science and Technology, Ramapuram,Chennai-89, India;
subhaagopi@gmail.com (R.S.)

Abstract: Skin cancer is a leading cause of cancer-related mortality, posing a significant global health challenge. Early detection and treatment are crucial for survival rates. While dermoscopy is a valuable non-invasive imaging tool for diagnosing skin lesions, its reliance on the expertise of dermatologists introduces variability, affecting diagnostic reliability. Existing deep learning models for skin lesion analysis often prioritize accuracy over computational efficiency, limiting their practical application in clinical settings where both rapidity and precision are crucial. To address these limitations, this study proposes a novel model called the Compact Fortified Weight-Prioritized Convolutional Network (CWCN), optimized using the Harbor Seal Whiskers Optimization (HOA) algorithm (CWCN-HOA-SLD-DI). The CWCN is designed to offer a balance between high performance and computational efficiency. Initially, dermoscopic images from the ISIC Archive dataset are collected and subjected to a series of preprocessing steps, including image augmentation to enhance robustness, normalization using log-sinh with Adaptive Box-Cox transformation, and noise removal employing Guided Box Filtering (GBF) and Guided Image Filtering (GIF). The CWCN-HOA framework is then utilized to classify skin lesions into categories such as Malignant, Melanocytic Nevus, Basal Cell Carcinoma, Actinic Keratosis, Benign Keratosis, Dermatofibroma, and Vascular Lesion. The proposed CWCN-HOA-SLD-DI model is implemented in Python, and its performance is evaluated against current methods. The results indicate that the CWCN-HOA approach achieves significant improvements in both classification accuracy as 99.98% and computational efficiency as 92ms. By offering a combination of high performance and computational efficiency, the CWCN-HOA model represents a promising solution for accurate and efficient skin cancer detection. Its potential to improve the diagnostic capabilities of dermatologists and enhance patient outcomes underscores its significance in addressing this critical global health issue.

Keywords: Compact Fortified Weight-Prioritized Convolutional Network, Dermoscopic images, Guided Box Filtering (GBF), Guided Image Filtering (GIF), Harbor Seal Whiskers Optimization (HOA) algorithm, Log-sinh with Adaptive Box-Cox transformation, Skin cancer, Skin lesion classification.

1. Introduction

Skin cancer is a leading cause of cancer-related mortality and poses a significant global health challenge [1-3]. According to the American Cancer Society, skin cancer mortality rates can reach as high as 75%, with melanoma showing the most alarming increase in incidence at 14% [4]. Early detection and treatment are crucial, as they significantly enhance survival rates [5]. Dermoscopy, a non-invasive imaging technique, is widely used in melanoma diagnosis [6-9]. Although it is superior to naked-eye examination, its accuracy heavily depends on the expertise and experience of dermatologists [10-13]. The inter-observer variability and diagnostic accuracy rates ranging from 75% to 84% underscore the need for supplementary diagnostic tools [14-16]. Leveraging artificial intelligence (AI)

for automated, non-contact melanoma diagnosis offers a promising solution [17-18]. However, challenges persist due to image interference factors, such as hair, skin preparation solutions, and auxiliary identification discs [19-20].

Accurate and timely identification of skin diseases is essential for effective dermatological management [21]. Previous research has explored automated skin lesion detection and classification using deep convolutional neural networks (CNNs) like VGG19 and ResNet152 on dermoscopic images [22-23]. While these approaches are innovative, they face challenges related to computational efficiency, accuracy, and explainability [24-26]. Balancing these aspects remains a significant hurdle, often preventing current methods from meeting real-time clinical requirements [27].

To address these challenges, a Compact Fortified Weight-Prioritized Convolutional Network (CWCN) optimized through the Harbor Seal Whiskers Optimization (HOA) algorithm is proposed. This model prioritizes computational efficiency without compromising accuracy. Here Compact Fortified Weight-Prioritized Convolutional Network (CWCN) are designed to efficiently extract relevant features from input data without requiring explicit segmentation and feature extraction process. This is achieved through their inherent architecture and training process. Unlike traditional machine learning methods, which rely on handcrafted features, deep learning models learn these features automatically, reducing the need for human intervention. This not only simplifies the modeling process but also improves computational efficiency, making lightweight CWCN models suitable for resource-constrained environments and real-time applications. The HOA enhances feature extraction and classification, addressing the limitations of existing models by offering a balance of accuracy, speed, and real-world applicability. The goal is to develop a highly efficient and accurate skin disease detection system. By combining a compact architecture, weight prioritization, and advanced optimization, the proposed method aims to surpass current solutions, providing a practical tool for dermatologists. The main contributions of this work are given below,

- It proposes a novel architecture called Compact Fortified Weight-Prioritized Convolutional Network (CWCN) for efficient and accurate skin lesion classification.
- Also, it employs Harbor Seal Whiskers Optimization (HOA) to enhance feature extraction and classification.
- It addresses the computational constraints by developing a lightweight model suitable for real-time applications in dermatological settings.
- It Improves the diagnostic accuracy by enhancing the precision and recall of skin cancer detection compared to existing methods.
- It provides a valuable tool for dermatologists to improve patient outcomes.

The subsequent sections of this manuscript present a comprehensive exploration of the proposed CWCN-HOA model. Section 2 provides a systematic review of existing skin lesion detection methods, highlighting their strengths and weaknesses. Section 3 delves into the methodological details of the CWCN-HOA model, elucidating its architecture and optimization process. Section 4 offers a rigorous evaluation of the model's performance, comparing it to state-of-the-art techniques. Finally, Section 5 provides a comprehensive discussion of the results, addressing limitations, and outlining potential future research directions.

2. Literature Survey

This section reviews recent advancements in deep learning approaches for automated skin lesion classification. Some of the recent related works are given below,

In 2023, Priyanka Pramila, R. and Subhashini, R., [21] introduced a fused deep convolutional neural network for automated skin lesion detection and classification using dermoscopic images (FDCNN-VGG19-ResNet152-SLD-DI). The process involved preprocessing images, followed by feature extraction using VGG19 and ResNet152 models. The extracted features were subsequently fed into a

fused deep convolutional neural network for classification. While achieving notable accuracy, the model's computational intensity limited its applicability in real-time scenarios.

In 2024, Anand, S., et.al [22] introduced an approach for classifying benign and malignant skin lesions based on dermoscopy images using a deep learning (DL) framework (DDNN-LACD-SLD-DI). It proposed a dual deep neural network (DDNN) to address the issue of varying classification accuracy across different classes. The DDNN comprised two distinct neural networks, each utilizing specific handcrafted feature sets called phase congruency (PC) and Gabor (GA) features. The outputs of these networks were combined using a likelihood-based add-and-compare decision (LACD) to enhance classification performance. While achieving commendable accuracy, the method incurred high computational time.

In 2022, Liu, Z., et.al [23] introduced the Clinical-Inspired Network (CI-Net) for automated skin lesion recognition (CI-Net-SLD-DI). This approach aimed to mimic the diagnostic process of human experts by incorporating three key modules like a lesion area attention module, a feature extraction module, and a lesion feature attention module. To further enhance discrimination, a distinguish module was added. Evaluated on multiple challenging datasets such as six challenging datasets, including ISIC 2016, ISIC 2017, ISIC 2018, ISIC 2019, ISIC 2020 and PH2 datasets, CI-Net demonstrated superior precision performance. However, the model's computational complexity presented a limitation for practical applications.

In 2022, Salma, W. and Eltrass, A.S., et.al [24] introduces Computer-Aided Diagnosis (CAD) system for accurately and efficiently classifying skin lesions. The proposed framework incorporated image preprocessing using morphological filtering to remove artifacts. Skin lesions were segmented via the GrabCut algorithm in the HSV color space. To mimic human diagnostic processes, an automated asymmetry, border irregularity, color and dermoscopic patterns (ABCD) rule implementation was integrated. Various pre-trained CNNs were evaluated, with ResNet50 combined with SVM demonstrating optimal performance. Data augmentation improved accuracy. While the system achieved promising results, its computational efficiency remains a challenge.

In 2023, Hameed, A., et.al [25] investigated automatic diagnosis and classification of skin lesions. This task is challenging due to factors like image variation, low contrast, and diverse lesion characteristics. The study initially focused on a binary classification, differentiating melanocytic lesions from normal skin. Subsequently, it tackled a more complex problem using the MNIST HAM10000 dataset, encompassing seven distinct skin cancer classes. To achieve this, it developed a stacked Convolutional Neural Network (CNN) model. By incorporating data augmentation and image preprocessing techniques, it achieves a classification accuracy of 95.2%. However, a high false-positive rate remains a concern.

In 2023, Bozkurt, F., et.al [26] proposes skin lesion classification combining effective data augmentation with a pre-trained Inception-Resnet-v2 deep learning model. The primary objective was to enhance skin cancer classification performance by augmenting the dataset using affine transformations and assessing its impact. After this, it developed a Inception-Resnet-v2 model for skin lesion identification. Results indicate a significant improvement in classification accuracy from 83.59% with the original dataset to 95.09% when employing the augmented dataset and the Inception-Resnet-v2 model. However, it has low precision.

In 2022, Nawaz, M., et.al [27] proposed a fully automated method for early-stage skin melanoma segmentation using a deep learning approach. A Faster Region-Based Convolutional Neural Network (R-CNN) combined with Fuzzy K-Means Clustering (FKM) is employed to process clinical images. Preprocessing steps for noise removal, illumination correction, and visual enhancement precede feature extraction using Faster R-CNN. Subsequently, FKM is applied to segment melanoma regions with varying sizes and boundaries. Evaluation on ISBI-2016, ISIC-2017, and PH2 datasets demonstrates superior performance compared to state-of-the-art methods, achieving average accuracies of 95.40%, 93.1%, and 95.6%, respectively. However, it has high False negative rate.

2.1. Problem Statement and Motivation

Accurate and timely skin disease detection is crucial for effective treatment outcomes. While dermoscopy is a valuable tool, its reliance on dermatologist expertise and the inherent variability between doctors hinder reliable diagnosis. Existing deep learning models for skin lesion analysis often prioritize accuracy over computational efficiency, limiting their applicability in real-world clinical settings [21-27]. This study addresses the need for a lightweight, high-performance model capable of accurate and rapid skin disease detection, thereby supporting dermatologists in providing timely and effective patient care.

3. Proposed Methodology for Swift Skin Lesion Identification

This section presents the Compact Fortified Weight-Prioritized Convolutional Network (CWCN) optimized by the Harbor Seal Whiskers Optimization (HOA) algorithm for Swift Skin Lesion Identification using Dermoscopic Images (CWCN-HOA-SLD-DI). A visual representation of the CWCN-HOA-SLD-DI methodology is provided in Figure 1. Subsequent sections offer a detailed examination of the constituent components of each stage.

3.1. Dataset Description

This section introduces the ISIC Archive, which serve as the foundation for developing and evaluating the CWCN-HOA-SLD-DI models for Swift Skin Lesion Identification using Dermoscopic Images. This ISIC Archive has extensive collection of over 100,000 high-quality dermoscopic images. It offers a vast collection of images, accurate ground truth annotations, a diverse range of skin lesion types, and regular updates, provides a valuable resource for developing and refining models capable of accurately identifying and classifying various skin lesions [28]. The dataset includes a wide range of skin lesions, such as melanoma, melanocytic nevi, basal cell carcinoma, actinic keratosis, benign keratosis, dermatofibroma, and vascular lesions.
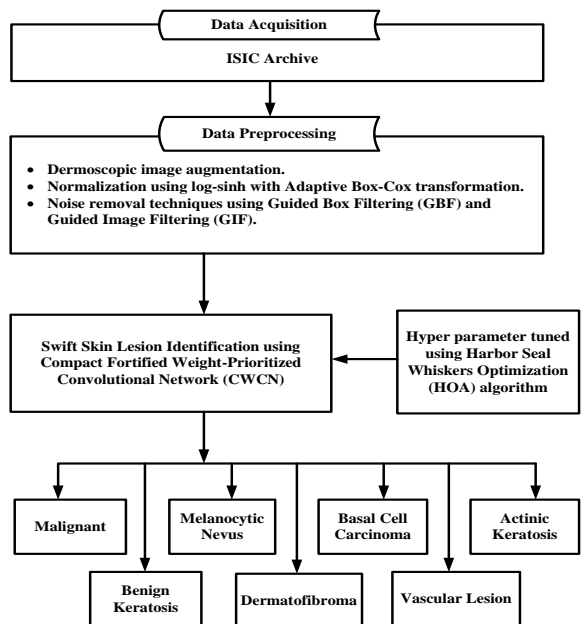

Figure 1.
Visual representation of the CWCN-HOA-SLD-DI methodology.

3.1. Dataset Description

This section introduces the ISIC Archive, which serve as the foundation for developing and evaluating the CWCN-HOA-SLD-DI models for Swift Skin Lesion Identification using Dermoscopic Images. This ISIC Archive has extensive collection of over 100,000 high-quality dermoscopic images. It offers a vast collection of images, accurate ground truth annotations, a diverse range of skin lesion types, and regular updates, provides a valuable resource for developing and refining models capable of accurately identifying and classifying various skin lesions [28]. The dataset includes a wide range of skin lesions, such as melanoma, melanocytic nevi, basal cell carcinoma, actinic keratosis, benign keratosis, dermatofibroma, and vascular lesions.

3.2. Pre-processing process

Generally, Pre-processing is a crucial step in skin lesion identification. It ensures dermoscopic image consistency, improves image quality, enhances feature extraction, and optimizes model performance. Techniques like normalization, noise reduction, and dermoscopic image augmentation are essential for preparing dermoscopic images for effective analysis.

Initially, the Dermoscopic image augmentation is an essential technique for enhancing the robustness and generalization capabilities of skin lesion identification models. By artificially increasing the diversity of the training dataset, augmentation helps models learn to recognize skin lesions under various conditions. Key augmentation techniques include Rotation to simulates different lesion orientations; Flipping for recognizing lesions from different perspectives; Scaling to handles variations in lesion size; Cropping and Zooming to focuses on specific lesion areas; Color Adjustments to accounts for different lighting conditions; Noise Injection to increases resilience to image artifacts and Elastic Deformations to recognizes lesions under slight skin surface changes. These techniques collectively enrich the training dataset, enabling the CWCN-HOA-SLD-DI model to more accurately and reliably identify skin lesions across diverse conditions.

After this, Normalization is a crucial preprocessing step in dermoscopic image analysis. It ensures standardized dermoscopic image, effectively manages outliers, maintains consistent feature scaling, and enhances model performance. The log-sinh with Adaptive Box-Cox transformation is particularly well-suited for this purpose, as it efficiently handles outliers, establishes a uniform distribution, and preserves essential image characteristics.

Here, the log-sinh transformation is specifically designed to handle zero values in image datasets, where pixel values typically range from 0 to 255. This transformation is defined in equation (1)

$$A_{DI} = log[sinh(DI + \varepsilon)] \tag{1}$$

where DI is the original dermoscopic image value and ε is a small constant added to prevent taking the logarithm of zero. Subsequently, the Adaptive Box-Cox transformation is applied to the log-sinh transformed dermoscopic image [29]. This transformation is defined in equation (2)

$$Normalization_{DI} = \begin{cases} ln(A_{DI} + \varepsilon); & if\ \lambda = 0 \\ \frac{(A_{DI}{}^{\lambda} - 1)}{\lambda}; & if\ \lambda \neq 0 \end{cases} \tag{2}$$

In this context, A_{DI} is the normalized dermoscopic image, $Normalization_{DI}$ is the log-sinh transformed dermoscopic image, and λ is the transformation parameter adaptively estimated for each feature to achieve optimal normalization. This two-step process effectively normalizes the dermoscopic image, ensuring it is prepared for robust analysis while preserving the inherent characteristics of dermoscopic images, leading to reliable and meaningful insights for skin lesion detection models.

Finally, a series of noise removal techniques were applied to the dermoscopic images to enhance image quality and consistency. For that, Guided Box Filtering (GBF) was employed to smooth the images while preserving critical edge details. The cumulative sums over the y-axis and a-axis were calculated using the following equations (3-4)

$$C(y,x) = C(y-1,x) + Itnsity(y + Radius) - Itnsity(y - Radius - 1, x)$$
(3)

$$D(y,x) = D(y, x-1) + C(y, x + Radius) - C(y, x - Radius - 1)$$
(4)

In this context, $C(y,x)$ and $D(y,x)$ represent the cumulative sums; $Itnsity$ denotes pixel intensity, and $Radius$ is the filter radius. The box filter output Box Filter (y, x) was calculated using equation (5)

$$\text{Box Filter } (y, x) = \frac{1}{(2Radius+1)^2} \times D(y,x)$$
(5)

After this, Guided Image Filtering (GIF) was applied to further refine the image, focusing on enhancing edge regions [30]. The output of GIF was calculated using equation (6)

$$\text{GIF} = \tilde{\alpha}^T \times Average_i + \tilde{\beta}$$
(6)

In this context, $\tilde{\alpha}$ and $\tilde{\beta}$ are averaged linear coefficients calculated using the following equations (7-8).

$$\tilde{\alpha} = \frac{1}{|Window|} \times \sum_{s \in Window} \alpha_s$$
(7)

$$\tilde{\beta} = \frac{1}{|Window|} \times \sum_{s \in Window} \beta_s$$
(8)

In this context, α_s and β_s are linear coefficients calculated using the following equations (9-10).

$$\alpha_s = (\textstyle\sum_s + \xi \times IdM)^{-1} \times \left(\frac{1}{|Window|} \times \sum_{i \in Window_s} Average_i \times IdM_i - \kappa_s \times \widetilde{Average}_s \right)$$
(9)

$$\beta_s = \left(\widetilde{Average}_s - \alpha_s^T \times \kappa_s \right)$$
(10)

In this context, IdM represents the Identity matrix. ξ represents the Controlling parameter. $\widetilde{Average}_s$ represents the Average of the input dermoscopic images. κ_s represents the Average of the guidance image. By combining box and guided filtering, the preprocessing effectively removed noise while preserving essential structural information, improving image quality, and preparing the dermoscopic images for subsequent deep learning analysis.

3.3. Swift Skin Lesion Identification using CWCN-HOA

After the pre-processed output, the next step is to utilize these CWCN-HOA model for the Swift Identification of Skin Lesion such as Malignant, Melanocytic Nevus, Basal Cell Carcinoma, Actinic Keratosis, Benign Keratosis, Dermatofibroma and Vascular Lesion. This section outlines the architecture and implementation details of the model, as well as the training and evaluation processes. The proposed CWCN framework for Swift Skin Lesion Identification consists of three prime units such as a Dermoscopic Feature Extractor for feature extraction from dermoscopic images, a deep Global Feature Aggregation Module for apprehending Contextual features, and a Decoder with Attention Mechanism. Skip networks are unified amongst the Dermoscopic Feature Extractor and Decoder with Attention Mechanism to reserve local features from dermoscopic images. The architecture of CWCN framework is given in Figure 2.

3.3.1. Dermoscopic Feature Extractor

Convolutional Neural Networks (CNNs) have consistently outperformed traditional image analysis methods, which are normally relied on manual engineered features, specifically when applied to the challenging task of skin lesion identification using dermoscopic images. In this work, the proposed CWCN Dermoscopic Feature Extractor is inspired by the SegNet architecture. It is adapted to decrease the parameter count from a substantial 14.7 million to a more efficient 583,070 for the improved

computational performance. The Dermoscopic Feature Extractor encompasses four processing units. Each unit comprises a series of convolutional layers, a downsampling layer, and a DropBlock regularization module. To align with the decoder's dimensions, the last unit eliminates the downsampling operation.

The Dermoscopic Feature Extractor's convolutional layers adopt the VGG architecture's configuration so it follows 3×3 filters with a stride of 1 for each layer. To enhance the capture of low-level features from dermoscopic images, each convolution stack encompasses two convolutional layers, followed by batch normalization and ReLU activation. It is expressed mathematically as shown in Equation (11).

$$\varrho\left(a_{y,CD}^{l}\right) = \max\left(0, a_{y,CD}^{l}\right) \qquad (11)$$

In this context, a^{l} represents the feature map at layer l, CD signifies the channel depth, while y represents the spatial dimensions. The ReLU activation function ϱ introduces non-linearity, enhancing the network's ability to learn complex patterns.

Each convolutional layer l generates an output feature map a_{y}^{l} by convolving the previous layer's feature maps Fm_{l} with corresponding kernels K and applying the activation function ϱ_{1} using equation (12)

$$a_{y}^{l} = \varrho_{1} \times \left[\sum_{CD^{*} \epsilon Fm_{l}} a_{CD^{*}}^{l-1} \times K_{CD^{*},CD}\right] \qquad (12)$$

Subsequently to prevent overfitting, DropBlock layer is introduced to regularize the network by randomly masking contiguous regions within feature maps [31]. To manage the substantial size of dermoscopic images, max-pooling is applied to downsample feature maps to reminisce crucial features.
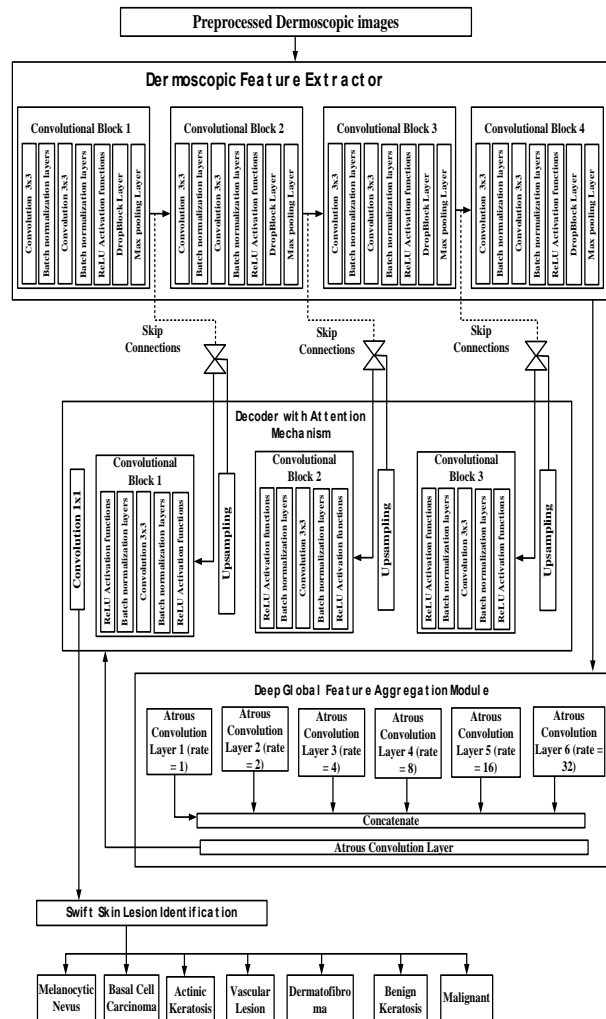
Figure 2.
CWCN architecture.

3.3.2. Deep Global Feature Aggregation Module

To counteract spatial information loss incurred by max-pooling and strided convolutions, the CWCN incorporates a Deep Global Feature Aggregation Module. This module utilizes atrous convolutions to expand the receptive field without increasing computational overhead. The atrous convolution operation defined as equation (13)

$$b\left[x\right] = \sum_{K=1}^{G} a[x + rate \times K] \times weight[K]$$

(13)

In this context, a rate parameter $rate$ is employed to control the dilation or stride of the convolution kernel $weight$. This mechanism effectively expands the kernel's receptive field without increasing its size $G \times G$, calculated as $G_d = K + (K-1)(rate - 1)$. Within the CWCN architecture, the Deep Global Feature Aggregation Module incorporates six layers with dilation rates ranging from $rate = 1\ to\ 32$. This conformation empowers the abstraction of deep-level features while conserving spatial resolution, decisive for precise skin lesion detection in dermoscopic images.

3.3.3. Decoder with Attention Mechanism

The CWCN's Decoder with Attention Mechanism enhances feature localization and suppresses false positives by incorporating an additive attention mechanism. This mechanism transfers information from the encoder to the decoder, selectively focusing on salient image regions. The attention coefficient μ_x within the range of 0 to 1 modulates the input feature maps using equation (14)

$$\widehat{a_{x,CD}^l} = a_{x,CD}^l * \mu_x^l$$
(14)

The attention coefficient μ_x^l is determined by combining encoder states with a Gating is applied prior to concatenation to selectively incorporate pertinent activations. Each pixel of dermoscopic images is represented by a feature vector a_x^l. A single scalar attention weight is calculated for each pixel of dermoscopic images. To capture the semantic context within dermoscopic images, multidimensional attention weights is employed. These weights, guided by an input vector gui_x determine the focus region for each pixel of dermoscopic images. The additive attention calculation is detailed in Equation (15-16).

$$q_{atn}^l = \gamma^T \left[\varrho \left[W_a^T \times a_x^l + W_{gui}^T \times gui_x + bias_{gui} \right] \right] + bias_\gamma$$
(15)

$$\mu_x^l = \varrho_2 \left[q_{atn}^l \left(a_x^l, gui_x; \Theta_{atn} \right) \right]$$
(16)

where W_a, W_{gui}, $bias_{gui}$, and Θ_{atn} are learnable parameters, gui_x is a feature vector from a lower layer, and sigmoid activation function is represented as $\varrho_2 = \frac{1}{1+exp(-a_{x,CD})}$. The vector gui originates from the network's lowest layer. This additive attention mechanism enhances feature representation and localization by selectively suppressing responses in irrelevant image areas, which is crucial for precise lesion identification. A fully connected layer follows the decoder, classifying each pixel within the feature map. The cross-entropy loss between the predicted and ground truth pixel-wise classifications is computed during training using equation (17)

$$Loss = -\frac{1}{Pixel} \sum_{Pixel}^{x=1} \sum_{U}^{CD=1} b_{CD,x} \times \ln\left(\widehat{b_{CD,x}}\right)$$
(17)

where $Pixel$ is the number of pixels, U is the number of Skin Lesion types such as Malignant, Melanocytic Nevus, Basal Cell Carcinoma, Actinic Keratosis, Benign Keratosis, Dermatofibroma and Vascular Lesion, $b_{CD,x}$ is the ground truth, and $\widehat{b_{CD,x}}$ is the predicted probability. The CWCN Network parameters are optimized through end-to-end training using backpropagation. The CWCN network's parameters require optimization to enhance its performance in skin lesion identification. Fine-tuning these parameters improves the network's accuracy in classifying dermoscopic images, leading to more reliable and effective diagnosis. The Harbor Seal Whiskers Optimization Algorithm (HOA) is a suitable choice for this task due to its ability to efficiently search the parameter space and find optimal solutions, thereby maximizing the CWCN network's performance.

3.4. Harbor Seal Whiskers Optimization Algorithm for Optimizing CWCN Network's Parameters

The Harbor Seal Whiskers Optimization Algorithm (HOA) is a metaheuristic inspired by the sensory capabilities of seal whiskers. The HOA algorithm offers several advantages, including its ability to effectively explore the search space, its computational efficiency, and its robustness to noise and local optima. These characteristics make it a suitable optimization method for various applications, including the optimization of the CWCN network's parameters. The HOA algorithm models the seal's prey-tracking behavior to optimize the CWCN network's parameters. The HOA algorithm consists of the following steps,

Step 1: Initialization

In Population initialization, arbitrarily create an initial population $Popu$ of M potential CWCN parameter sets, where each CWCN parameter set R_i represents a candidate solution.

Step 2: Fitness Evaluation

In this step, fitness function $Fitness\ Function\ (R_i)$ is defined to evaluate the quality of each CWCN parameter set R_i that considers the CWCN network's performance on a validation dataset.

Step 3: Sensing velocity calculation

In this, the sensing velocity Vel_i for each CWCN parameter set is calculated using the following equation (18)

$$Vel_i = \frac{SF}{2\pi} \times \frac{(2Pos_i{}^2 - Dist^2)}{(Pos_i{}^2 + Dist^2)^{\frac{5}{2}}}$$

(18)

In this context, Vel_i is the sensing velocity of CWCN parameter set R_i, Pos_j is the seal's position, $Dist$ is the distance to prey, SF is a scaling factor using equation (19)

$$SF = 2\pi \times \omega \times Amp \times Osc \times Ti$$

(19)

Where ω is angular frequency, Amp is displacement amplitude, Osc is oscillating sphere diameter, and Ti is time.

Step 4: Sensing velocity update

In this, the sensing velocity Vel_i based on the CWCN parameter set's fitness is updated using equation (20)

$$Vel_i^{l+1} = Ellipse \times R_1 \times Vel_i^l + v \times \vartheta \times R_2 \left[Global\ P_{Ideal} - Pos_i^l \right] + u \times \vartheta \times R_3 \left[Local\ P_{Ideal,i} - Pos_i^l \right]$$

(20)

In this context, Vel_i^{l+1} is the updated sensing velocity, $Ellipse$ is the ellipse diameter using equation (21)

$$Ellipse = uv * \frac{1}{\sqrt{v^2 \times \sin^2 \times \vartheta + u^2 \times \cos^2 \times \vartheta}}$$

(21)

In this context, R_1, R_2, and R_3 are random numbers, $Global\ P_{Ideal}$ and $Local\ P_{Ideal,i}$ represent global and local best positions, ϑ is the water flow attack angle, u and v are ellipse axis lengths using equation (22-23)

$$u = 0.14 \times \sin(0.92 \times nbr + 1.5 \times \pi) + 1$$

(22)

$$v = 0.067 \times \sin(0.91 \times nbr + \pi) - 0.0041 \times nbr + 0.64$$

(23)

In this context, nbr is the number of whisker cross-sections [32].

Step 5: Position Update

In this, the CWCN parameter set R_i based on its sensing velocity is updated using equation (24)

$$Pos_i^{l+1} = Pos_i^l + Vel_i^{l+1}$$

(24)

In this context, Pos_i^{l+1} is the updated position of the CWCN parameter set R_i.

Step 6: Termination

The HOA algorithm terminates when a stopping criterion is met, such as a maximum number of iterations or a satisfactory fitness value. The pseudocode of HOA algorithm is given in Algorithm 1.

Algorithm 1: Pseudocode of HOA Algorithm for CWCN network's parameters

Randomly generate an initial population of potential CWCN parameter sets.

Evaluate the quality of each CWCN parameter set using a fitness function that considers the CWCN network's performance on a validation dataset.

Assign a sensing velocity to each CWCN parameter set using equation (18-19).

Update the sensing velocity of each CWCN parameter set based on its performance using equation (20-23)

Update the CWCN parameter set positions based on the new sensing velocity using equation (24)

Iteratively refine CWCN parameter sets until the termination criteria are met.

4. Results and Discussion

In this, performance of the Compact Fortified Weight-Prioritized Convolutional Network optimized with Harbor seal whiskers optimization algorithm for Swift Skin Lesion Identification using Dermoscopic Images is estimated (CWCN-HOA-SLD-DI) in this section. Here Skin Dermatography image is segmentated into 3:1:1 distribution for training, validation, and testing. The experimental setup encompassed an Intel Core i7 processor with 2.50 GHz, 8 GB RAM, Windows 10 operating system. The CWCN-HOA-SLD-DI method is implemented in Python programming environment. This section presents a comprehensive evaluation and comparison of the proposed CWCN-HOA-SLD-DI framework against conventional approaches FDCNN-VGG19-ResNet152-SLD-DI [21], DDNN-LACD-SLD-DI [22] and CI-Net-SLD-DI [23] respectively. The output result of CWCN-HOA-SLD-DI method is given in Figure 3.

4.1. Performance Metrics

Here the various performance metrics are given below into the following section,

4.1.1. Accuracy

It represents the ratio of correct predictions to total predictions. It is premeditated through equation (25)

$$Accuracy = \frac{TP+TN}{TP+FP+TN+FN}$$

(25)

Where True Positive (TP) denote accurate positive predictions; True Negative (TN) specify accurate negative predictions; False Positive (FP) epitomize incorrect positive predictions; False Negative (FN) imply incorrect negative predictions.

4.1.2. Precision

It indicates the proportion of positive predictions that were correct. It is premeditated through equation (26)

$$Precision = \frac{TP}{(TP+FP)}$$

(26)

4.1.2. Recall

It measures the proportion of actual positives identified correctly. It is premeditated through equation (27)

$$Recall = \frac{TP}{(TP+FN)}$$

(27)

4.1.3. F1 Score
It represents the harmonic mean of precision and recall. It is premeditated through equation (28)

$$F1\ Score = \frac{2\times(Precision\times Recall)}{(Precision+Recall)}$$

(28)
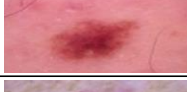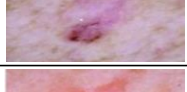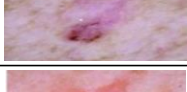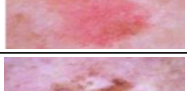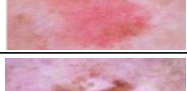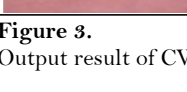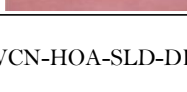
Input Image	Pre-processing Output	Classification Output
		Malignant
		Melanocytic Nevus
		Basal Cell Carcinoma
		Actinic Keratosis
		Benign Keratosis
		Dermatofibroma
		Vascular Lesion

Figure 3.
Output result of CWCN-HOA-SLD-DI method.

4.1.4. False Positive Rate (FPR)
It indicates the proportion of negative instances incorrectly classified as positive. It is premeditated through equation (29)

$$FPR = \frac{FP}{(FP+TN)}$$

(29)

4.1.5. False Negative Rate (FNR)
It indicates the proportion of positive instances incorrectly classified as negative. It is premeditated through equation (30)

$$FNR = \frac{FN}{(TP+FN)}$$

(30)

4.1.6. Specificity
It measures the proportion of actual negatives correctly identified. It is premeditated through equation (31)

$$\text{Specificity} = \frac{TN}{(TN+FP)}$$

(31)

4.1.7. Execution time

It represents the computational resource consumption of the model. Typically measured in seconds or milliseconds.

4.2. Performance Analysis

The Figure 4-11 offers a comparative analysis of the proposed CWCN-HOA-SLD-DI framework against conventional approaches FDCNN-VGG19-ResNet152-SLD-DI [21], DDNN-LACD-SLD-DI [22] and CI-Net-SLD-DI [23] respectively.
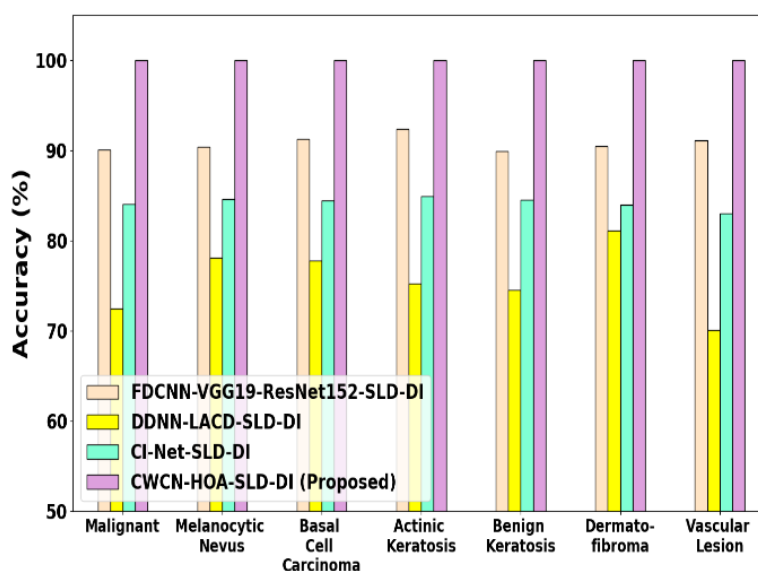

Figure 4.
Accuracy analysis.

Figure 4 presents the accuracy analysis for diverse types of Skin Lesion using the proposed CWCN-HOA-SLD-DI method. The proposed CWCN-HOA-SLD-DI method attains 11.03%, 37.99% and 18.95% higher accuracy for Melanoma analysis against conventional approaches like FDCNN-VGG19-ResNet152-SLD-DI, DDNN-LACD-SLD-DI, and CI-Net-SLD-DI respectively. For Melanocytic Nevus analysis, it attains 10.68%, 28.06% and 18.24% higher accuracy in comparison with the same conventional approaches. Basal Cell Carcinoma analysis expresses an accuracy increase of 9.61%, 28.6% and 18.41% over the same conventional approaches. The accuracy for Actinic Keratosis analysis improves by 8.26%, 32.94% and 17.73% contrary to the methods FDCNN-VGG19-ResNet152-SLD-DI, DDNN-LACD-SLD-DI, and CI-Net-SLD-DI respectively. For Benign Keratosis analysis, it attains 11.18%, 34.16% and 18.27% higher accuracy in comparison with the same conventional approaches. Dermatofibroma analysis expresses an accuracy increase of 10.55%, 23.27% and 19.16% over the same conventional approaches. Lastly, for Vascular Lesion analysis, the method attains an accuracy enhancement of 9.72%, 42.64% and 20.42% when compared to the conventional approaches. This extensive accuracy analysis validates the superior performance of the proposed CWCN-HOA-SLD-DI method across all types of Skin Lesion Identification.
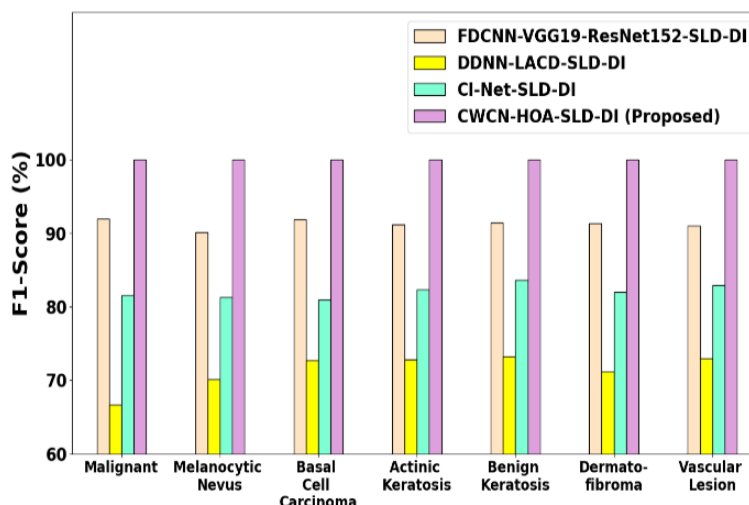
Figure 5.
F1-Score analysis.

Figure 5 presents the F1-Score analysis for diverse types of Skin Lesion using the proposed CWCN-HOA-SLD-DI method. The proposed CWCN-HOA-SLD-DI method attains 8.77%, 50.01% and 22.59% higher F1-Score for Melanoma analysis against conventional approaches like FDCNN-VGG19-ResNet152-SLD-DI, DDNN-LACD-SLD-DI, and CI-Net-SLD-DI respectively. For Melanocytic Nevus analysis, it attains 11.02%, 42.71% and 23.02% higher F1-Score in comparison with the same conventional approaches. Basal Cell Carcinoma analysis expresses an F1-Score increase of 8.82%, 37.506% and 23.59% over the same conventional approaches. The F1-Score for Actinic Keratosis analysis improves by 9.74%, 37.33% and 21.45% contrary to the methods FDCNN-VGG19-ResNet152-SLD-DI, DDNN-LACD-SLD-DI, and CI-Net-SLD-DI respectively. For Benign Keratosis analysis, it attains 9.35%, 36.608% and 19.61% higher F1-Score in comparison with the same conventional approaches. Dermatofibroma analysis expresses an F1-Score increase of 9.52%, 40.56% and 22.005% over the same conventional approaches. Lastly, for Vascular Lesion analysis, the method attains an F1-Score enhancement of 9.88%, 37.07% and 20.62% when compared to the conventional approaches. These results underscore the superior performance of the CWCN-HOA-SLD-DI method in accurately identifying and classifying various skin lesions.
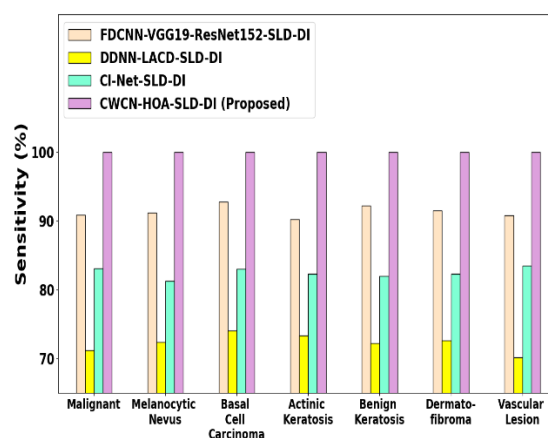

Figure 6.
Sensitivity analysis.

Figure 6 presents a sensitivity analysis of diverse skin lesion types using the proposed CWCN-HOA-SLD-DI method. Compared to conventional approaches such as FDCNN-VGG19-ResNet152-SLD-DI, DDNN-LACD-SLD-DI, and CI-Net-SLD-DI, the CWCN-HOA-SLD-DI method demonstrates superior sensitivity in identifying skin lesions. Specifically, the proposed method achieves high sensitivity rates of 10.03%, 40.55%, and 20.36% for Melanoma; 9.69%, 38.15%, and 23.04% for Melanocytic Nevus; 7.78%, 34.99%, and 20.48% for Basal Cell Carcinoma; 10.805%, 36.37%, and 21.57% for Actinic Keratosis; 8.42%, 38.44%, and 21.99% for Benign Keratosis; 9.32%, 37.66%, and 21.47% for Dermatofibroma; and 10.16%, 42.59%, and 19.82% for Vascular Lesion. These findings underscore the CWCN-HOA-SLD-DI method's efficacy in accurately detecting various skin lesions across different levels of severity.

Figure 7 presents a precision analysis of diverse skin lesion types using the proposed CWCN-HOA-SLD-DI method. Compared to conventional approaches such as FDCNN-VGG19-ResNet152-SLD-DI, DDNN-LACD-SLD-DI, and CI-Net-SLD-DI, the CWCN-HOA-SLD-DI method demonstrates superior performance in accurately identifying skin lesions across varying severities. The proposed CWCN-HOA-SLD-DI method attains 7.51%, 59.47% and 24.83% high precision for Melanoma analysis; 12.35%, 47.27% and 23.001% high precision for Melanocytic Nevus analysis; 9.85%, 40.01% and 26.704% high precision for Basal Cell Carcinoma analysis; 8.68%, 38.29% and 21.34% high precision for Actinic Keratosis analysis; 10.29%, 34.77% and 17.23% high precision for Benign Keratosis; 9.71%, 43.45% and 22.53% high precision for Dermatofibroma analysis; 9.59%, 31.55% and 21.42% high precision for Vascular Lesion analysis; when compared to the conventional approaches like FDCNN-VGG19-ResNet152-SLD-DI, DDNN-LACD-SLD-DI, and CI-Net-SLD-DI respectively. These results highlight the CWCN-HOA-SLD-DI method's effectiveness in distinguishing between different skin lesion types with precision.
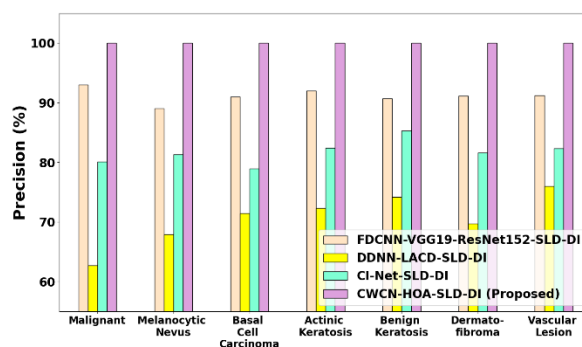

Figure 7.
Precision analysis.

Figure 8 presents the Specificity analysis for diverse types of Skin Lesion using the proposed CWCN-HOA-SLD-DI method. The proposed CWCN-HOA-SLD-DI method attains 22.52%, 49.22% and 23.43% high Specificity for Melanoma analysis; 21.95%, 44.92% and 20.48% high Specificity for Melanocytic Nevus analysis; 14.908%, 35.09% and 26.54% high Specificity for Basal Cell Carcinoma analysis; 26.56%, 36.97% and 19.03% high Specificity for Actinic Keratosis analysis; 21.93%, 38.87% and 20.46% high Specificity for Benign Keratosis; 21.46%, 40.82% and 21.93% high Specificity for Dermatofibroma analysis; 24.92%, 38.88% and 25% high Specificity for Vascular Lesion analysis compared to the conventional approaches like FDCNN-VGG19-ResNet152-SLD-DI, DDNN-LACD-SLD-DI, and CI-Net-SLD-DI respectively. These results highlight the CWCN-HOA-SLD-DI method's ability to accurately identify true negative cases across various skin lesion categories.
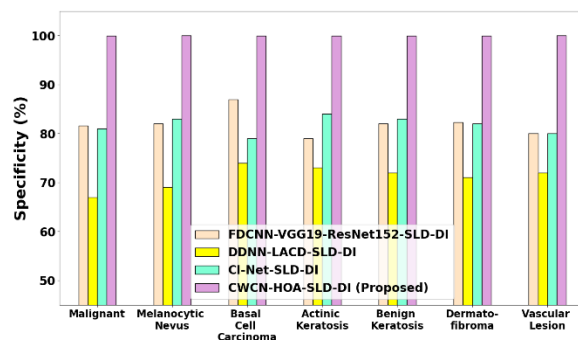
Figure 8.
Specificity analysis.

Figure 9 illustrates the false positive rate (FPR) associated with the proposed CWCN–HOA–SLD–DI model in the context of skin lesion classification. In comparison to conventional approaches such as FDCNN-VGG19-ResNet152-SLD-DI, DDNN-LACD-SLD-DI, and CI-Net-SLD-DI, the CWCN–HOA-SLD-DI method exhibits a lower FPR as 99.92%, 99.95% and 99.93%, indicating the proportion of benign skin lesions that are incorrectly classified as malignant by the model. A lower FPR indicates better model performance in avoiding false alarms.
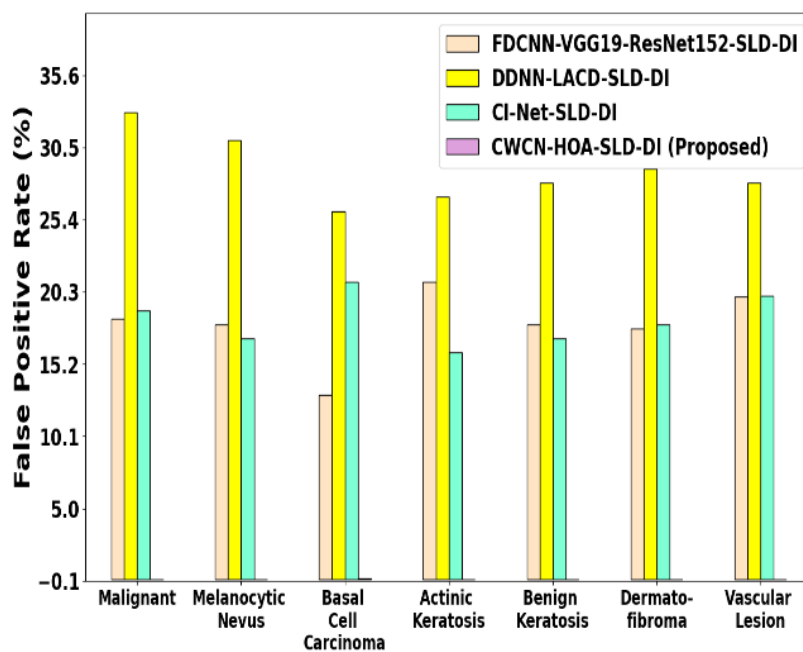

Figure 9.
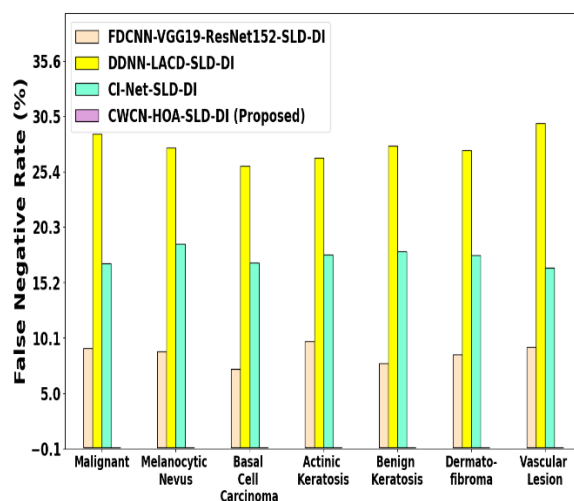False positive rate (FPR) analysis.

Figure 10.
False negative rate (FPR) analysis.

Figure 10 also presents the false negative rate (FNR) associated with the proposed CWCN-HOA-SLD-DI model for skin lesion classification. In comparison to conventional approaches such as FDCNN-VGG19-ResNet152-SLD-DI, DDNN-LACD-SLD-DI, and CI-Net-SLD-DI, the CWCN-HOA-SLD-DI method exhibits a lower FNR as 99.86%, 99.95% and 99.93%, signifies the proportion of malignant skin lesions that are incorrectly classified as benign. A lower FNR implies enhanced model sensitivity in detecting malignant cases.
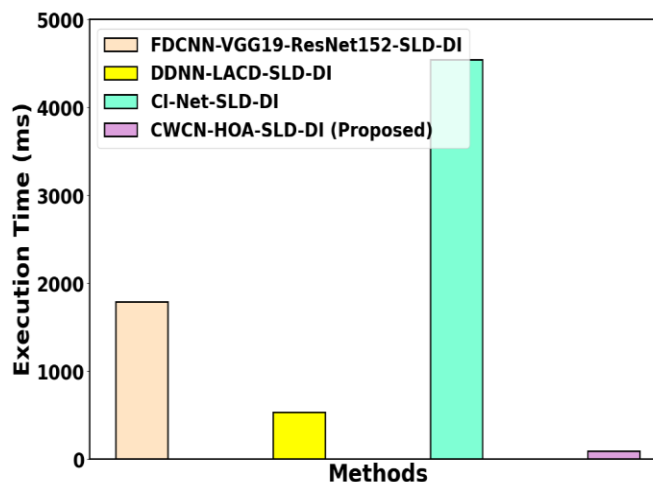

Figure 11.
Execution time analysis.

Figure 11 presents a comparative analysis of execution time for various skin lesion types using the proposed CWCN-HOA-SLD-DI method and conventional approaches like FDCNN-VGG19-ResNet152-SLD-DI, DDNN-LACD-SLD-DI, and CI-Net-SLD-DI. The proposed method demonstrates significantly reduced computational cost, achieving 94.85%, 82.77%, and 97.97% lower execution times compared to the respective conventional methods. This substantial improvement in processing speed highlights the computational efficiency of the CWCN-HOA-SLD-DI model, making it a practical choice for real-world applications requiring rapid skin lesion analysis.

4.3. Discussion

The proposed Compact Fortified Weight-Prioritized Convolutional Network (CWCN) optimized with the Harbor Seal Whiskers Optimization (HOA) algorithm (CWCN-HOA-SLD-DI) demonstrates promising results from Figure 4-11 and Table 1 for skin lesion classification using dermoscopic images.

Table 1.
Overall evaluation metrics analysis.

Performance metrics/methods	FDCNN-VGG19-ResNet152-SLD-DI	DDNN-LACD-SLD-DI	CI-Net-SLD-DI	CWCN-HOA-SLD-DI (Proposed)
Accuracy (%)	90.78	75.60429	84.20857	99.98857
Sensitivity (Recall) (%)	91.35143	72.26629	82.46943	99.98857
Specificity (%)	81.99571	71.14286	81.71429	99.988
Precision (%)	91.14771	70.6	81.70571	99.98857
F1-Score (%)	91.24245	71.35785	82.07087	99.98857
False positive rate (%)	18.00429	28.85714	18.28571	0.012
False negative rate (%)	8.648571	27.73371	17.53057	0.011429
Latency (ms)	1789	534	4543	92

The CWCN-HOA-SLD-DI model achieves significantly higher accuracy as 10.14%, 32.25% and 18.73% and F1-score as 9.58%, 40.12% and 21.83% compared to conventional methods across various skin lesion categories. The model also exhibits enhanced sensitivity as 9.45%, 38.36% and 21.24% and precision as 9.69%, 41.62% and 22.37%, suggesting its effectiveness in accurately detecting both malignant and benign lesions while minimizing misclassifications. Lower False Positive Rates (FPR) as 99.92%, 99.95% and 99.93%, and False Negative Rates (FNR) as 99.86%, 99.95% and 99.93% signify the model's ability to avoid false alarms and accurately identify true negative and positive cases, respectively. High Specificity values as 21.94%, 40.54% and 22.36% indicate the model's capability to accurately identify true negative cases across various skin lesions. The CWCN-HOA-SLD-DI model demonstrates significantly reduced execution time as 94.85%, 82.77%, and 97.97% compared to conventional approaches like FDCNN-VGG19-ResNet152-SLD-DI, DDNN-LACD-SLD-DI, and CI-Net-SLD-DI respectively. This makes it a practical solution for real-world clinical applications demanding rapid skin lesion analysis.

Future research will focus on expanding the model's capabilities and applicability. Training the model with a larger and more diverse dataset enhance its generalizability, while multi-center validation studies strengthen its clinical relevance. By addressing these areas, the CWCN-HOA-SLD-DI model has the potential to become a valuable tool for dermatologists in early and accurate skin cancer detection, ultimately contributing to improved patient outcomes.

5. Conclusion

The CWCN-HOA-SLD-DI model represents a significant advancement in automated skin lesion classification. By effectively combining the Compact Fortified Weight-Prioritized Convolutional Network with the Harbor Seal Whiskers Optimization algorithm, the model achieves a remarkable balance between diagnostic accuracy and computational efficiency. This dual advantage positions the model as a transformative tool in dermatology. Its robustness, demonstrated through extensive testing on the ISIC Archive dataset, ensures consistent and reliable results across diverse lesion types. Moreover, the model's adaptability to various clinical environments paves the way for widespread implementation, making early detection and treatment more accessible globally. The CWCN-HOA-SLD-DI model achieves 10.14%, 32.25% and 18.73% high accuracy; 9.45%, 38.36% and 21.24% high sensitivity; 21.94%, 40.54% and 22.36% high Specificity; 9.69%, 41.62% and 22.37% high precision;

9.58%, 40.12% and 21.83% high F1-score; 99.92%, 99.95% and 99.93% low False Positive Rates (FPR); 99.86%, 99.95% and 99.93% low False Negative Rates (FNR) and 94.85%, 82.77%, and 97.97% lower execution times compared to conventional approaches like FDCNN-VGG19-ResNet152-SLD-DI, DDNN-LACD-SLD-DI, and CI-Net-SLD-DI respectively. In Future research will focus on expanding the model's training data and validating its performance across multiple clinical centers to confirm its generalizability. Additionally, exploring integration with other diagnostic tools would further enhance its utility in comprehensive skin cancer management. By this, the CWCN-HOA-SLD-DI model has the potential to significantly improve clinical outcomes in skin cancer care. Its continued development would play a crucial role in reducing the global burden of skin cancer, highlighting the importance of AI-driven solutions in modern healthcare.

Copyright:

References

[1] Varma, P.B.S., Paturu, S., Mishra, S., Rao, B.S., Kumar, P.M. and Krishna, N.V., 2022. SLDCNet: Skin lesion detection and classification using full resolution convolutional network-based deep learning CNN with transfer learning. Expert Systems, 39(9), p.e12944.

[2] Manikandan, G., Hung, B.T., Shankar, S.S. and Chakrabarti, P., 2023. Enhanced ai-based machine learning model for an accurate segmentation and classification methods. International Journal on Recent and Innovation Trends in Computing and Communication, 11, pp.11-18.

[3] Karunkuzhali, D., Geetha, D., Manikandan, G., Manikandan, J. and Kavitha, V., 2022, November. Artificial Intelligence and Advanced Technology based Bridge Safety Monitoring System. In 2022 Sixth International Conference on I-SMAC (IoT in Social, Mobile, Analytics and Cloud)(I-SMAC) (pp. 631-634). IEEE.

[4] Maqsood, S. and Damaševičius, R., 2023. Multiclass skin lesion localization and classification using deep learning based features fusion and selection framework for smart healthcare. Neural networks, 160, pp.238-258.

[5] Bhuvaneswari, G. and Manikandan, G., 2018. A novel machine learning framework for diagnosing the type 2 diabetics using temporal fuzzy ant miner decision tree classifier with temporal weighted genetic algorithm. Computing, 100, pp.759-772.

[6] Ahammed, M., Al Mamun, M. and Uddin, M.S., 2022. A machine learning approach for skin disease detection and classification using image segmentation. Healthcare Analytics, 2, p.100122.

[7] Sultanuddin, S.J., Kumar, A.G.D., Maithili, K., Vanguri, G.N., Padhi, M.K., Gangopadhyay, A., Bhuvaneswari, G. and Manikandan, G., 2024. A Novel Support Vector Machine based Improved Aquila Optimizer-based Text Mining Mechanism for the Healthcare Applications. Journal of Electrical Systems, 20(5s), pp.2909-2920.

[8] Khan, M.A., Sharif, M.I., Raza, M., Anjum, A., Saba, T. and Shad, S.A., 2022. Skin lesion segmentation and classification: A unified framework of deep neural network features fusion and selection. Expert Systems, 39(7), p.e12497.

[9] Suresh, G., Bhuvaneswari, G., Manikandan, G. and Shanthakumar, P., 2024. Chronological bald eagle optimization based deep learning for image watermarking. Expert Systems with Applications, 238, p.121545.

[10] Bian, X., Pan, H., Zhang, K., Li, P., Li, J. and Chen, C., 2022. Skin lesion image classification method based on extension theory and deep learning. Multimedia Tools and Applications, 81(12), pp.16389-16409.

[11] Bhuvaneswari, G. and Manikandan, G., 2019. An intelligent intrusion detection system for secure wireless communication using IPSO and negative selection classifier. Cluster Computing, 22(Suppl 5), pp.12429-12441.

[12] Shahsavari, A., Khatibi, T. and Ranjbari, S., 2023. Skin lesion detection using an ensemble of deep models: SLDED. Multimedia Tools and Applications, 82(7), pp.10575-10594.

[13] Benyahia, S., Meftah, B. and Lézoray, O., 2022. Multi-features extraction based on deep learning for skin lesion classification. Tissue and Cell, 74, p.101701.

[14] Bhuvneswari, G. and Manikandan, G., 2019. Recognition of ancient stone inscription characters using histogram of oriented gradients. In Proceedings of International Conference on Recent Trends in Computing, Communication & Networking Technologies (ICRTCCNT).

[15] Dillshad, V., Khan, M.A., Nazir, M., Saidani, O., Alturki, N. and Kadry, S., 2023. D2LFS2Net: Multi-class skin lesion diagnosis using deep learning and variance-controlled Marine Predator optimisation: An application for precision medicine. CAAI Transactions on Intelligence Technology.

[16] Manikandan, G. and Srinivasan, S., 2013. An efficient algorithm for mining spatially co-located moving objects. American Journal of Applied Sciences, 10(3), pp.195-208.

[17] Alhudhaif, A., Almaslukh, B., Aseeri, A.O., Guler, O. and Polat, K., 2023. A novel nonlinear automated multi-class skin lesion detection system using soft-attention based convolutional neural networks. Chaos, Solitons & Fractals, 170, p.113409.

[18] Anand, V., Gupta, S., Nayak, S.R., Koundal, D., Prakash, D. and Verma, K.D., 2022. An automated deep learning models for classification of skin disease using Dermoscopy images: A comprehensive study. Multimedia Tools and Applications, 81(26), pp.37379-37401.

[19] Geetha, D., Kavitha, V., Manikandan, G. and Karunkuzhali, D., 2021, July. Enhancement and Development of Next Generation Data Mining Photolithographic Mechanism. In Journal of Physics: Conference Series (Vol. 1964, No. 4, p. 042092). IOP Publishing.

[20] Yue, G., Wei, P., Zhou, T., Jiang, Q., Yan, W. and Wang, T., 2022. Toward multicenter skin lesion classification using deep neural network with adaptively weighted balance loss. IEEE Transactions on Medical Imaging, 42(1), pp.119-131.

[21] Priyanka Pramila, R. and Subhashini, R., 2023. Automated skin lesion detection and classification using fused deep convolutional neural network on dermoscopic images. Computational Intelligence, 39(6), pp.1073-1087.

[22] Anand, S., Sheeba, A. and Maha Tharshini, M.K., 2024. Relative likelihood based aggregated dual deep neural network for skin lesion recognition in dermoscopy images. Multimedia Tools and Applications, pp.1-24.

[23] Liu, Z., Xiong, R. and Jiang, T., 2022. CI-Net: Clinical-inspired network for automated skin lesion recognition. IEEE Transactions on Medical Imaging, 42(3), pp.619-632.

[24] Salma, W. and Eltrass, A.S., 2022. Automated deep learning approach for classification of malignant melanoma and benign skin lesions. Multimedia Tools and Applications, 81(22), pp.32643-32660.

[25] Hameed, A., Umer, M., Hafeez, U., Mustafa, H., Sohaib, A., Siddique, M.A. and Madni, H.A., 2023. Skin lesion classification in dermoscopic images using stacked convolutional neural network. Journal of Ambient Intelligence and Humanized Computing, 14(4), pp.3551-3565.

[26] Bozkurt, F., 2023. Skin lesion classification on dermatoscopic images using effective data augmentation and pre-trained deep learning approach. Multimedia Tools and Applications, 82(12), pp.18985-19003.

[27] Nawaz, M., Mehmood, Z., Nazir, T., Naqvi, R.A., Rehman, A., Iqbal, M. and Saba, T., 2022. Skin cancer detection from dermoscopic images using deep learning and fuzzy k-means clustering. Microscopy research and technique, 85(1), pp.339-351.

[28] ISIC-archive "https://challenge.isic-archive.com/data/", accessed in August 2024.

[29] Rahman, M., Al-thubaiti, S., Breitenfeldt, R.W., Jiang, J., Light, E.B., Molenaar, R.H., Patwary, M.S.A. and Wuollet, J.A., 2016. A note on adaptive Box-Cox transformation parameter in linear regression. Research and Scientific Innovation Society RSIS International.

[30] Kumar, M.P., Poornima, B., Nagendraswamy, H.S. and Manjunath, C., 2021. Structure-preserving NPR framework for image abstraction and stylization. The Journal of Supercomputing, 77(8), pp.8445-8513.

[31] Munir, F., Azam, S., Jeon, M., Lee, B.G. and Pedrycz, W., 2021. LDNet: End-to-end lane marking detection approach using a dynamic vision sensor. IEEE Transactions on Intelligent Transportation Systems, 23(7), pp.9318-9334.

[32] Zaher, H., Al-Wahsh, H., Eid, M.H., Gad, R.S., Abdel-Rahim, N. and Abdelqawee, I.M., 2023. A novel harbor seal whiskers optimization algorithm. Alexandria Engineering Journal, 80, pp.88-109.